

Received 10 May 2020; revised 3 June 2020; accepted 6 June 2020. Date of publication 9 June 2020; date of current version 22 June 2020.

Digital Object Identifier 10.1109/OJAP.2020.3001087

# Dual Circularly Polarized Aperture Array Antenna in Gap Waveguide for High-Efficiency Ka-Band Satellite Communications

MIGUEL FERRANDO-ROCHER<sup>ID</sup> (Member, IEEE), JOSE IGNACIO HERRANZ-HERRUZO<sup>ID</sup> (Member, IEEE), ALEJANDRO VALERO-NOGUEIRA<sup>ID</sup> (Senior Member, IEEE), AND BERNARDO BERNARDO-CLEMENTE

Instituto de Telecommunicaciones y Aplicaciones Multimedia, Universitat Politècnica de València, 46022 Valencia, Spain

CORRESPONDING AUTHOR: M. FERRANDO-ROCHER (e-mail: miferrroc@iteam.upv.es)

This work was supported by the Spanish Ministry of Economy and Competitiveness (Ministerio de Economía y Competitividad) under Project TEC2016-79700-C2-1-R.

**ABSTRACT** A novel fully metallic Ka-band dual circularly polarized antenna array is presented in this contribution. It consists of 64 circular apertures ( $8 \times 8$ ) and it is implemented in gap waveguide technology. The antenna includes 4 layers, which are completely metallic, leading to a highly efficient performance. The experimental results confirm reflection coefficient values lower than  $-10$  dB from 29 GHz to 31 GHz as well as stable radiation patterns throughout the whole frequency range. Good average axial ratio (AR) of 1.5 dB has been measured in the working band for both polarizations. Measured directivity is 28 dBi and antenna efficiency keeps close to 80%.

**INDEX TERMS** Array antenna, dual circular polarization, gap waveguide, Ka-band.

## I. INTRODUCTION

IN RECENT years, the demand for satellite capacity has grown similarly to other wired and cellular wireless communication systems, and the market trend is to increase the service throughput speeds in at least one order of magnitude compared to existing Ku-band systems. Demand for Ka-band satellite capacity is expected to grow over the next years [1]. High-throughput satellites (HTS) provide global broadband multimedia services to fixed and mobile users. For fixed service, reflector antennas remain a reliable option being a cost-effective solution. Nevertheless, for on-the-move communications, reflectors may not be the best choice due to their high profile. Consequently, in aeronautical and land mobile sectors, there is a strong demand for lightweight, highly efficient and low-profile antennas. As revealing piece of information, the European Space Agency has funded more than 180 projects during the 2000s and 2010s for the development of satellite communications (SATCOM) within ARTES program.

In fairness, it should be highlighted that the ultimate goal would be the development of Ka-band phased arrays with full-electronic beam scanning. In this way, the antenna would be so versatile that it should reconfigure dynamically its

polarization and beam pointing. Nevertheless, due to system complexity, cost, and energy consumption, there is not yet a cost-competitive commercial antenna of that kind, at least to the knowledge of these authors. Until such technology becomes a plausible option, there exists an interest in halfway solutions using different approaches: parabolic reflectors, reflectarrays, transmitarrays, lenses, horns or waveguide arrays. These type of antennas, widely developed and studied, are able to meet some of the SATCOM requirements, being one of them the dual circular polarization (CP) performance.

One of the most successful solutions to achieve high-gain dual circularly polarized antennas is a reflectarray, where the contributions made by Encinar group [2] stand out. Other approaches can be found in the recent literature regarding transmitarrays [3], horn arrays [4]–[5] and waveguide arrays [6]. It is worth mentioning here a Ka-band waveguide array using additive manufacturing [7], which is promising in terms of cost, weight, volume and antenna efficiency.

This work proposes a novel approach to attain a highly efficient dual circularly polarized antenna, specially devoted to Ka-band satellite communications. It should be noted that in the case of on-the-move applications, this fixed-beam

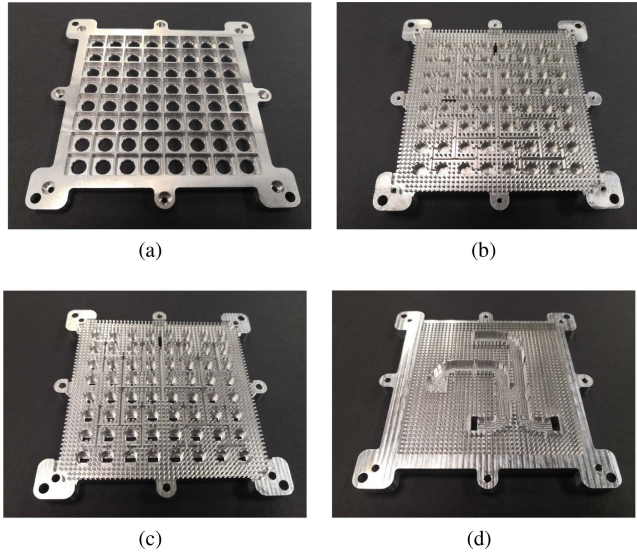


**FIGURE 1.** The 4 metallic layers making up the antenna: (a) Top Lid, (b) V-Pol Layer, (c) H-Pol layer and (d) Hybrid coupler.

antenna would need to be embarked on a mechanical tracking system.

Here the development initiated in [8] is culminated. The objective has been to achieve the dual-circular-polarization performance from a dual linearly-polarized antenna. To this end, an hybrid coupler has been designed, manufactured and integrated in the lower part of the antenna. As a result, a 4-layer low-profile antenna made entirely of aluminum and fully based on gap waveguide (GW) technology is presented (Fig. 1).

Next sections show the design and experimental measurements of the proposed antenna. Section II focuses on presenting the design of the Riblet-type coupler needed for polarization conversion. Section III displays the measured performance of the dual circularly-polarized antenna. Finally, the paper concludes highlighting the most relevant contributions of this work.

## II. RIBLET-TYPE COUPLER DESIGN

The antenna is composed of four stacked aluminum pieces. The first of these pieces hosts a novel Riblet-type coupler implemented in GW. The remaining three pieces that make up the antenna are, in ascending order, the feeding, coupling and radiation layers, which were previously presented in [8].

### A. PREVIOUS DESIGN CONSIDERATIONS

The gap-waveguiding concept is based on controlling the propagation of electromagnetic waves along desired directions inside a parallel-plate waveguide by using fundamentals of boundary conditions and canonical surfaces [9].

One of the variants of this technology is the Groove Gap Waveguide (GGW), whose modal behavior is practically identical to that of a rectangular waveguide (RW). So, the preliminary hybrid design was based on RW to later replace the lateral metallic walls by the bed of nails of GW technology. The ability to replace RW with GGW while retaining

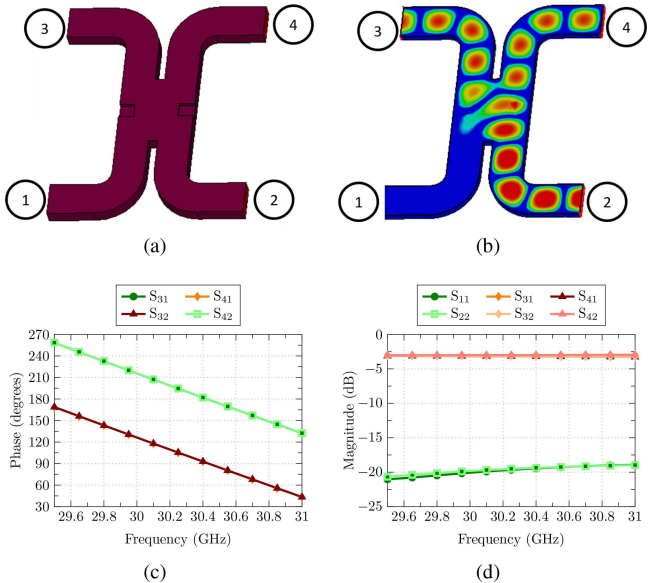


**FIGURE 2.** Riblet coupler design with RW: (a) Basic structure; (b) Electric field magnitude showing the coupler performance; (c) Phase and (d) magnitude of the simulated S-parameters.

similar characteristics was demonstrated in [10]. Thus, the RW model simplifies the geometry of the structure and reduces the computational cost of a full-wave optimization process.

The proposed coupler is a modification of the Riblet's short-slot coupler [11]. It presents a compact aspect with a 3-dB coupling factor that is attainable by a central H-plane cavity to which four arms are attached as the input/output ports. It is common that, starting from the coupler described by Riblet, tuning elements such as septums or slits are added to improve the device response according to the given specifications. Fig. 2 shows the geometrical structure of the directional coupler designed using RW. Simulated response is shown in Figs. 2(c) and 2(d).

This hybrid directional coupler has been designed to operate in Ka band from 29.5 GHz to 31 GHz. This range corresponds to the working band of the antenna to which the hybrid will be connected [8], so a wider frequency bandwidth is not sought. Fig. 2(b) shows the electric field when port 2 is excited. The figure shows that the field from the input port (port 2) is divided equally between the two output ports (3 and 4) with 90° phase-shift. As can be seen, the signal barely enters the isolated port 1. Fig. 2(c) shows graphically the 90° phase-difference between ports 3 and 4. Finally, Fig. 2(d) shows that the reflection coefficient keeps close to -20 dB throughout the band.  $S_{31}$ ,  $S_{41}$ ,  $S_{32}$ , and  $S_{42}$ -parameters remain around -3dB, as expected.

### B. GAP WAVEGUIDE RIBLET-TYPE COUPLER

Once the preliminary coupler is designed in RW, the device is converted to GW technology. Fig. 3 shows a top view of the hybrid layout, as well as its most relevant dimensions. Notice that now the feeding port is no longer placed on the same plane as the waveguide, but at the back of the piece

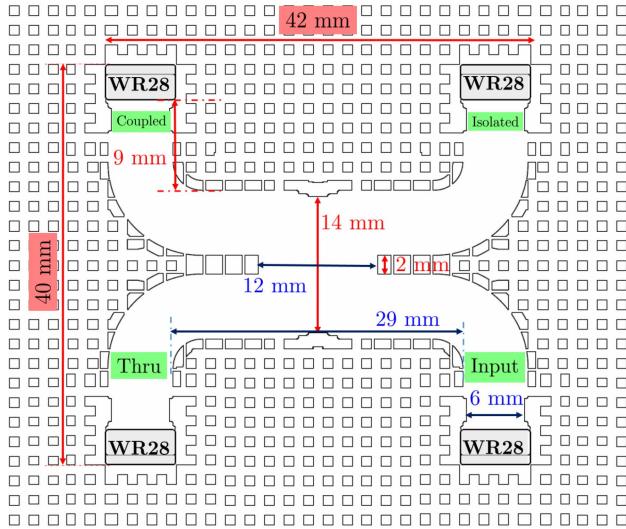


**FIGURE 3.** Layout of Riblet-type coupler in gap waveguide.

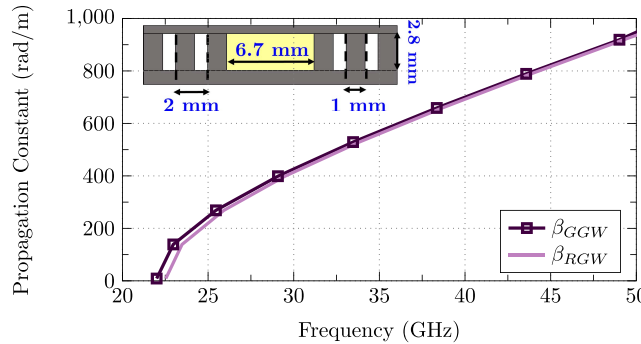


**FIGURE 4.** Comparison between the propagation constant in the waveguide using GGW and RW. Cross-section of RW is marked in yellow.

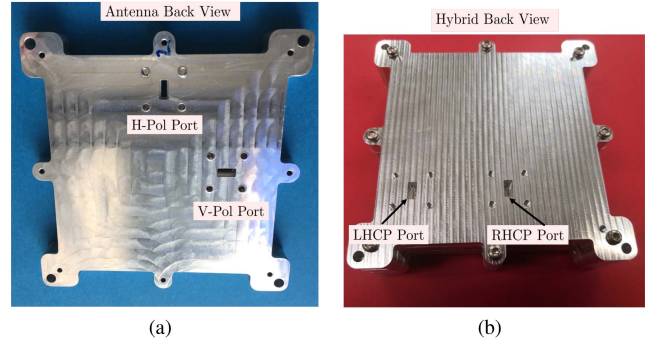
by using WR-28 flanges. Besides that, the small notch used in the central part of the RW hybrid has been re-optimized adopting a stepped shape in the new GGW design. The rest of the dimensions, such as the height (2.8 mm) and width (6 mm) of the GGW, are identical to those of the RW design.

Fig. 4 shows the dispersion curve of the proposed hybrid using GGW or RW. This graph shows that the propagation constant is almost identical in both cases, which manifests the equivalence between the two waveguides (GGW and RW).

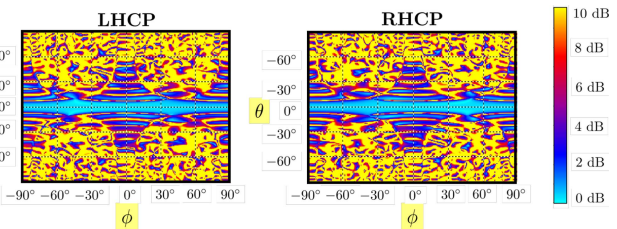
### C. COUPLER MODIFICATION FOR CP CONVERSION

Once the coupler is designed in Gap Waveguide, the next step is connecting it to the dual linearly-polarized antenna [8] from its back. However, this antenna from a previous project was not initially designed to be connected to any additional parts. Therefore the two input ports are close to the two sidewalls and even more, they are rotated 90° with respect to each other, which is an added problem to connect antenna and coupler.

Figs. 5(a) and 5(b) show pictures of the rear of the antenna and the back side of the manufactured hybrid metallic piece,



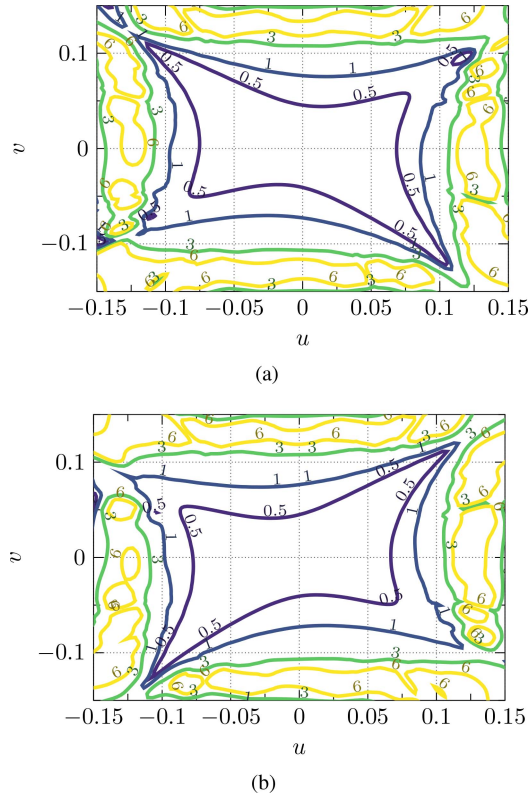
**FIGURE 5.** (a) Rear part of the antenna, (b) rear part of the hybrid and (c) x-ray view showing the connection between the hybrid and the antenna.



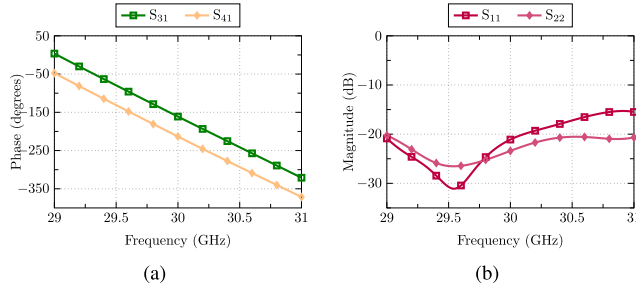
**FIGURE 6.** Simulated performance of the axial ratio for different  $\phi$ -cut planes versus  $\theta$  angle.

where both input ports are pointed out. Finally, Fig. 5(c) shows how it is possible to connect the hybrid to the antenna. This connection has important considerations.

The new added arms (Fig. 5(c)) connecting the hybrid to the antenna input ports are now of different length. It is therefore evident a 90° phase-difference between both output ports cannot be expected. This has been done on purpose. Measurements in [8] revealed that the phase difference in broadside direction between V-Pol and H-Pol field components was of  $-140^\circ$  at the central frequency (30.25 GHz). However right-hand CP (RHCP) would need  $-90^\circ$  phase difference instead. Thus, when RHCP port is excited, the V-Pol port must be fed with a phase increment of  $+50^\circ$  with respect to the H-pol port.



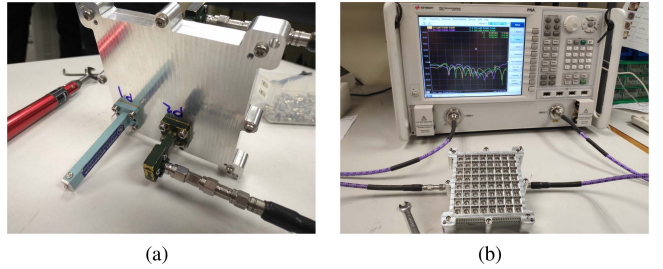
**FIGURE 7.** Contour plot of simulated axial ratio in u-v plane: (a) LHCP and (b) RHCP. ( $u = \sin \theta \cos \phi$ ,  $v = \sin \theta \sin \phi$ .)



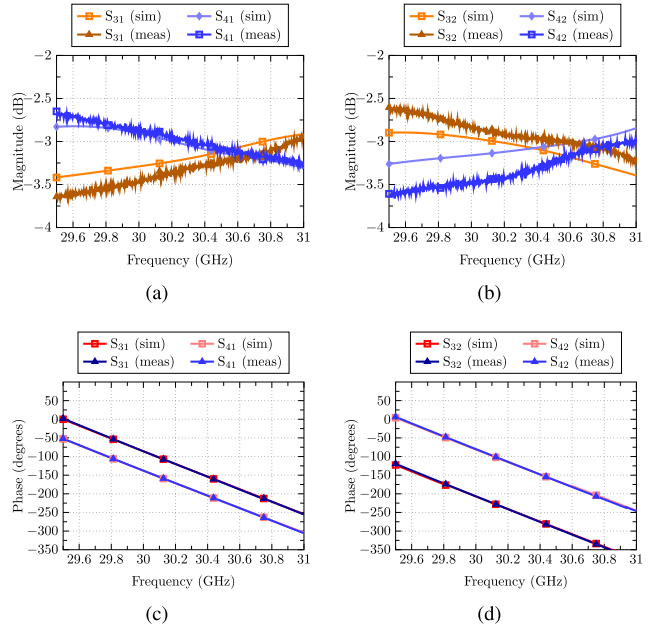
**FIGURE 8.** Simulated S-parameters of the modified hybrid.

Fig. 6 shows the simulated axial ratio (AR) at 30 GHz when the dual linearly-polarized antenna is properly connected to the proposed hybrid. Both the RHCP and LHCP axial ratio is shown in Fig. 6. In addition, Fig. 7 depicts a 2D contour plot showing the AR of each polarization in the u/v coordinate space. These figures demonstrate a good purity of the dual circular polarization in the main beam, which will be confirmed in the experimental measurements section.

Simulated S-parameters of the new hybrid can be observed in Figs. 8(a) and 8(b). The graph shows that the additional waveguide paths behave as expected, providing required 50° phase-difference between ports 3 and 4 (Fig. 8(a)), instead of original 90° (Fig. 5(c)). As for the magnitude of the S-parameters, the new added arms break the structure symmetry of the prior Riblet-type design. As a consequence,



**FIGURE 9.** Photographs during the S-parameters measurement process: (a) hybrid and (b) fully-assembled antenna.



**FIGURE 10.** Measured S-parameters of the modified hybrid.

**TABLE 1.** Design specifications.

Frequency Band	Gain	Antenna Eff.	AR	Pol.
29.5-31 GHz	27 dBi	75%	$\leq 3$ dB	Dual-Circular

S<sub>11</sub>- and S<sub>22</sub>-parameters are not identical any more, but they still keep lower than  $-16$  dB within the band of interest, as shown in Fig. 8(b).

#### D. EXPERIMENTAL VALIDATION OF THE COUPLER

In first place, the coupler has been measured separately by using a dedicated cover, before assembling it to the complete antenna. A photograph taken during the S-parameter measurement process is shown in Fig. 9.

Fig. 10 shows a comparison of the measured and simulated S-parameters of the coupler. Figs. 10(a) and 10(b) reveal that the power imbalance between ports is slightly higher when compared to simulation. Figs. 10(c) and 10(d), however, manifests a perfect agreement between measured and simulated phase of S-parameters.

### III. ANTENNA MEASUREMENTS

Finally, once the hybrid has been manufactured and experimentally validated, the next step is to assemble it to the

**TABLE 2.** Comparison of the proposed dual circularly-polarized array with previously published works.

Dual Circularly-Pol Array	Number of elements	Band	Tech.	Gain	Efficiency
[12]	2 x 2	L	$\mu$ trip	$\approx 9$ dBi	n/a
[13]	4 x 4	X, Ku	$\mu$ trip	$\approx 17$ dBi	n/a
[14]	1 x 4	Ka	SIW	$\approx 12$ dBi	$\approx 50\%$
[15]	1 x 7	Ka	$\mu$ trip	$\approx 11$ dBi	n/a
[16]	16 x 16	Ka	RW	$\approx 31$ dBi	$\approx 60\%$
[17]	8 x 8	V	SIW	$\approx 25$ dBi	$\approx 70\%$
[18]	15 x 15	W	SIW	$\approx 25$ dBi	$\approx 58\%$
<b>This work</b>	<b>8 x 8</b>	<b>Ka</b>	<b>GW</b>	$\approx 27$ dBi	$\approx 75\text{-}80\%$

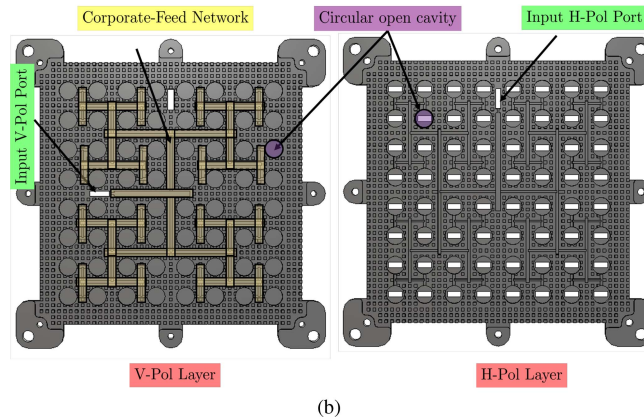
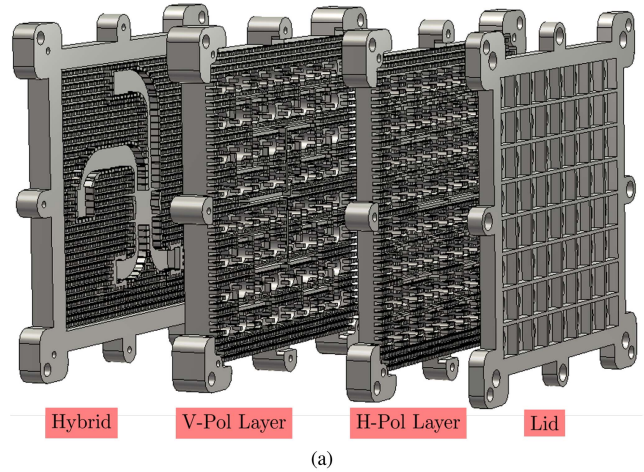


**FIGURE 11.** (a) Exploded side view of the full antenna and (b) top view of the two feeding layers.

antenna described in [8]. Fig. 11(a) shows a side view of the complete antenna. A top view indicating the fundamental parts of the distribution network and the radiating elements is shown in Fig. 11(b). Then, the complete antenna is measured. Keep in mind that there are two input ports, one providing RHCP and the other LHCP. Table 1 highlights the design specifications being pursued.

Experimental measurements of the dual linearly-polarized antenna in [8] did show a reflection coefficient with some frequency ranges slightly above  $-10$  dB. Now, this fact has been fixed thanks to a proper optimization of the hybrid considering the actual antenna S-parameters. As noted in Figs. 12(a) and 12(c), the reflection coefficient is now below

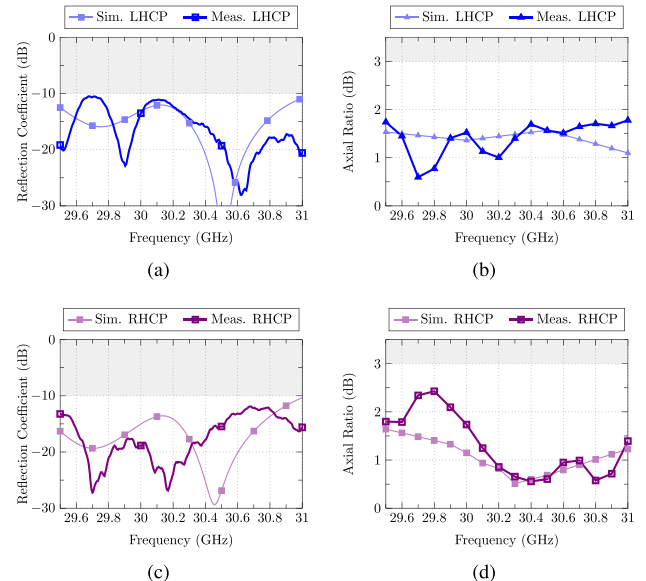


**FIGURE 12.** Antenna measurements: (a) reflection coefficient (LHCP), (b) axial ratio (LHCP), (c) reflection coefficient (RHCP) and (d) axial ratio (RHCP).

the desired  $-10$  dB from 29.5 GHz to 31 GHz for both ports. The simulated and measured curves do not match perfectly but they show a similar trend. It can be seen how the minimum  $S_{11}$  at 30.5 GHz in LHCP has shifted slightly to higher frequencies, whereas the RHCP measured curve has apparently moved to lower frequencies.

As for polarization purity, the measured AR values are shown in Figs. 12(b) and 12(d). AR remains below 2 dB for LHCP port in the whole band. In the RHCP case, AR reaches a peak value of 2.5 dB at 29.8 GHz. It is worth stressing that a good average AR of 1.5 dB has been measured in the working band for both polarizations.

Fig. 13 plots the main measured antenna parameters, such as gain and antenna efficiency. High efficiency, above 75%, is achieved in the whole band, as expected for an antenna formed entirely of aluminum pieces. The figures also include the simulated gain and antenna efficiency for the sake of comparison. In both cases, great agreement in gain values is observed between 30 GHz and 31 GHz. High antenna efficiency has been observed in simulation, around 90%. This value has been confirmed with the experimental measurement, which is bordering on 80%. This slight deviation between both, simulation and measurement may be due to

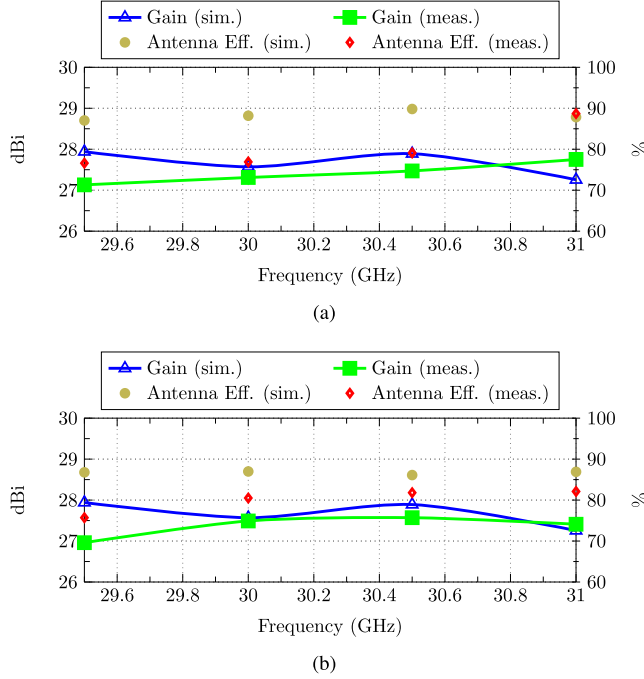


**FIGURE 13.** Measured gain (left axis), and antenna efficiency (right axis): (a) LHCP and (b) RHCP.

surface roughness. The measured radiation patterns along both main cuts are shown in Fig 14. A great stability of radiation patterns within the entire bandwidth, from 29.5 GHz to 31 GHz, is achieved.

Table 2 provides a comparative summary of the performance of this contribution with recently published dual circularly-polarized antennas. The table reveals that the proposed antenna stands out for its high efficiency. This antenna cannot compete in terms of lightness and weight with microstrip antennas, but it is a more suitable solution in the millimeter-wave band where dielectric losses are critical. Compared to other full-metal antennas, as the one published in [16], this contribution is much more compact and has a simpler and less voluminous corporate-feed network. Precisely by using fewer transitions and layers, 4 in total instead of 7, it is possible to achieve better antenna efficiency.

#### IV. CONCLUSION

A dual circularly-polarized Ka-band aperture array antenna using Gap Waveguide technology is presented. The design, integration and assembly of a novel hybrid coupler with a dual linearly-polarized antenna has allowed us to provide a prototype with attractive features for SATCOM on-the-move applications, such as high efficiency and low profile. From the authors' knowledge, it is the first completely metallic antenna implemented in GW with dual-circular-polarization radiation capability. Nevertheless, there are some appealing aspects yet to explore, such as synthesizing a tapered aperture distribution to reduce the sidelobes and properly meet mask regulations.

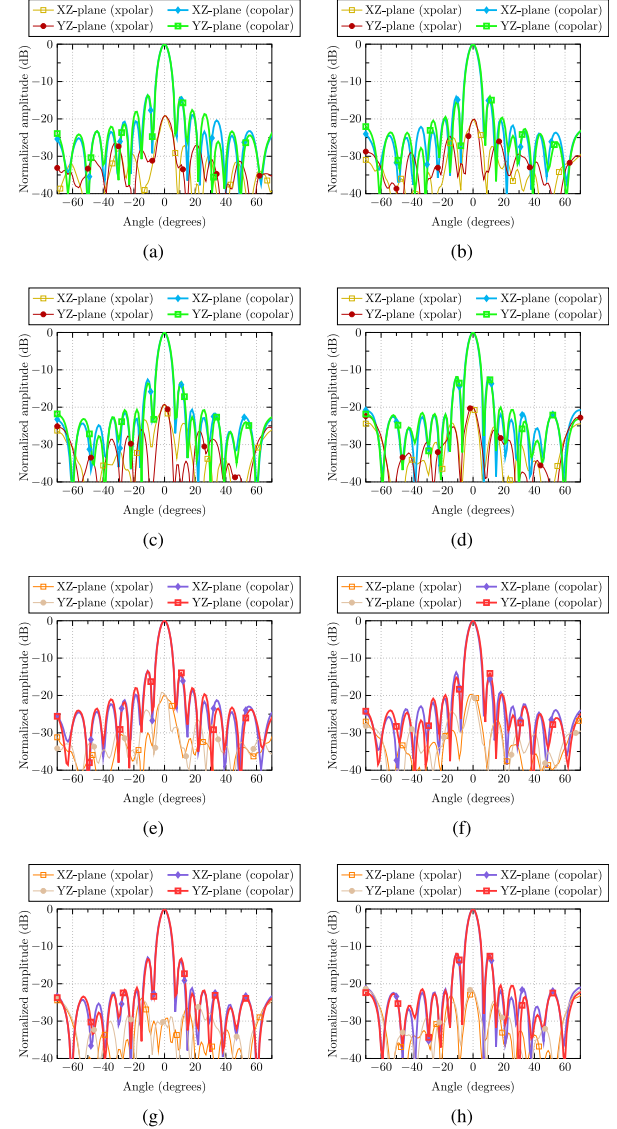


**FIGURE 14.** Normalized measured XZ-plane and YZ-plane radiation patterns for several frequencies with LHCP performance (Port 1): (a) 29.5 GHz, (b) 30 GHz, (c) 30.5 GHz, (d) 31 GHz, and RHCP performance (Port 2): (e) 29.5 GHz, (f) 30 GHz, (g) 30.5 GHz, (h) 31 GHz.

#### REFERENCES

- [1] M. Ferrando-Rocher, "Gap waveguide array antennas and corporate-feed networks for mm-Wave band applications," Ph.D. dissertation, Dept. de Comun., Universitat Politècnica de València, Valencia, Spain, 2018.
- [2] D. Martinez-de Rioja, R. Florencio, J. A. Encinar, E. Carrasco, and R. R. Boix, "Dual-frequency reflectarray cell to provide opposite phase shift in dual circular polarization with application in multibeam satellite antennas," *IEEE Antennas Wireless Propag. Lett.*, vol. 18, pp. 1591–1595, 2019.
- [3] P. Naseri, S. A. Matos, J. R. Costa, C. A. Fernandes, and N. J. Fonseca, "Dual-band dual-linear-to-circular polarization converter in transmission mode application to k/ka-band satellite communications," *IEEE Trans. Antennas Propag.*, vol. 66, no. 12, pp. 7128–7137, Dec. 2018.
- [4] R. V. Gatti and R. Rossi, "A dual circularly polarized slot-fed horn array antenna with linear polarization-tracking feature," *Int. J. RF Microw. Comput.-Aided Eng.*, vol. 28, no. 9, 2018, Art. no. e21480.
- [5] C. Shu *et al.*, "A wideband dual-circular-polarization horn antenna for mmWave wireless communications," *IEEE Antennas Wireless Propag. Lett.*, vol. 18, pp. 1726–1730, 2019.

- [6] J. I. Herranz-Herruzo, A. Valero-Nogueira, M. Ferrando-Rocher, B. Bernardo, A. Vila, and R. Lenormand, "Low-cost Ka-band switchable RHCP/LHCP antenna array for mobile SATCOM terminal," *IEEE Trans. Antennas Propag.*, vol. 66, no. 5, pp. 2661–2666, May 2018.
- [7] F. Bongard, M. Gimersky, S. Doherty, X. Aubry, and M. Krummen, "3D-printed Ka-band waveguide array antenna for mobile SATCOM applications," in *Proc. 11th Eur. Conf. Antennas Propag. (EUCAP)*, Paris, France, 2017, pp. 579–583.
- [8] M. Ferrando-Rocher, J. I. Herranz-Herruzo, A. Valero-Nogueira, B. Bernardo-Clemente, A. U. Zaman, and J. Yang, "8×8 Ka-band dual-polarized array antenna based on gap waveguide technology," *IEEE Trans. Antennas Propag.*, vol. 67, no. 7, pp. 4579–4588, Jul. 2019.
- [9] E. Rajo-Iglesias, M. Ferrando-Rocher, and A. U. Zaman, "Gap waveguide technology for millimeter-wave antenna systems," *IEEE Commun. Mag.*, vol. 56, no. 7, pp. 14–20, Jul. 2018.
- [10] M. Ferrando-Rocher, A. Valero-Nogueira, J. I. Herranz-Herruzo, A. Berenguer, and B. Bernardo-Clemente, "Groove gap waveguides: A contactless solution for multilayer slotted-waveguide array antenna assembly," in *Proc. 10th Eur. Conf. Antennas Propag. (EuCAP)*, Davos, Switzerland, 2016, pp. 1–4.
- [11] H. J. Riblet, "The short-slot hybrid junction," *Proc. IRE*, vol. 40, no. 2, pp. 180–184, Feb. 1952.
- [12] H. Li, X. Du, J. Y. Yin, J. Ren, and Y. Yin, "Differentially-fed dual-circularly polarized antenna with slow-wave delay lines," *IEEE Trans. Antennas Propag.*, vol. 68, no. 5, pp. 4066–4071, May 2020.
- [13] J.-D. Zhang, W. Wu, and D.-G. Fang, "Dual-band and dual-circularly polarized shared-aperture array antennas with single-layer substrate," *IEEE Trans. Antennas Propag.*, vol. 64, no. 1, pp. 109–116, Jan. 2016.
- [14] Q. Wu, J. Hirokawa, J. Yin, C. Yu, H. Wang, and W. Hong, "Millimeter-wave multibeam endfire dual-circularly polarized antenna array for 5G wireless applications," *IEEE Trans. Antennas Propag.*, vol. 66, no. 9, pp. 4930–4935, Sep. 2018.
- [15] Y.-H. Yang, B.-H. Sun, and J.-L. Guo, "A low-cost, single-layer, dual circularly polarized antenna for millimeter-wave applications," *IEEE Antennas Wireless Propag. Lett.*, vol. 18, no. 4, pp. 651–655, Apr. 2019.
- [16] J. Wu, Y. J. Cheng, H. B. Wang, Y. C. Zhong, D. Ma, and Y. Fan, "A wideband dual circularly polarized full-corporate waveguide array antenna fed by triple-resonant cavities," *IEEE Trans. Antennas Propag.*, vol. 65, no. 4, pp. 2135–2139, Apr. 2017.
- [17] Y. Zhao and K.-M. Luk, "Dual circular-polarized SIW-fed high-gain scalable antenna array for 60 GHz applications," *IEEE Trans. Antennas Propag.*, vol. 66, no. 3, pp. 1288–1298, Mar. 2018.
- [18] Y. J. Cheng, J. Wang, and X. L. Liu, "94 GHz substrate integrated waveguide dual-circular-polarization shared-aperture parallel-plate long-slot array antenna with low sidelobe level," *IEEE Trans. Antennas Propag.*, vol. 65, no. 11, pp. 5855–5861, Nov. 2017.



**JOSE IGNACIO HERRANZ-HERRUZO** (Member, IEEE) was born in Valencia, Spain, in 1978. He received the undergraduate degree in telecommunication engineering from the Universitat Politècnica de València, Valencia, in 2002, where he is currently pursuing the Ph.D. degree. In 2002, he joined the Departamento de Comunicaciones, Universitat Politècnica de València, where he is currently an Associate Professor. His current research interests include the optimization of waveguide slot array antennas and efficient computational methods for planar structure.



**ALEJANDRO VALERO-NOGUEIRA** (Senior Member, IEEE) was born in Madrid, Spain, in 1965. He received the undergraduate degree in telecommunication engineering from the Universidad Politécnica de Madrid, Madrid, in 1991, and the Ph.D. degree in telecommunication from the Universitat Politècnica de València, Valencia, Spain, in 1997. In 1992, he joined the Departamento de Comunicaciones, Universitat Politècnica de València, where he is currently a Full Professor. In 1999, he was on leave with the ElectroScience Laboratory, Ohio State University, Columbus, OH, USA, where he was involved in fast solution methods in electromagnetics (EMs) and conformal antenna arrays. His current research interests include computational EMs, waveguide slot arrays, gap waveguides, theory of characteristic modes, and automated antenna design procedures.



**BERNARDO BERNARDO-CLEMENTE** was born in Valencia, Spain, in 1972. He received the undergraduate degree in telecommunication engineering from the Universitat Politècnica de València, Valencia, in 2003, where he is currently pursuing the Ph.D. degree in telecommunication. Since 2005, he has been with the Instituto de Telecommunicaciones y Aplicaciones Multimedia, Universitat Politècnica de València. His current research interests include antenna measurement, antenna fabrication, and near-to-far-field transformation.



**MIGUEL FERRANDO-ROCHER** (Member, IEEE) was born in Alcoy, Spain. He received the M.Sc. and Ph.D. degrees in telecommunication engineering from the Universitat Politècnica de València (UPV), Valencia, Spain, in 2012 and 2018, respectively. In 2012, he joined the Complex Radiation Systems Team, Institute of Electronics and Telecommunications, Rennes, France, as a Researcher, where he was involved in reflect array antennas for satellite applications in collaboration with Thales Alenia Space, Paris, France. In 2016, he joined the Chalmers University of Technology, Gothenburg, Sweden, as a Guest Researcher. Since 2013, he has been with the Electromagnetic Radiation Group, Institute of Telecommunications and Multimedia Applications, UPV. Since September 2019, he has been an Assistant Professor with the Department of Physics, Systems Engineering and Signal Theory, University of Alicante. His research activity is also developed in the microwave and electromagnetism group. His current research interests include satellite communication on-the-move, high-gain antennas and arrays, gap waveguide technology, and millimeter-wave components. He was a recipient of the AIRBUS Defence and Space Award in 2019, the URSI Conference Best Student Paper Award in 2017, and the Jury Prize and the Audience Prize for the best thesis project of the II Meeting of Ph.D. Students at UPV. He received an Erasmus Grant to study at Ghent University, Ghent, Belgium, in 2010.